A voltage and frequency droop control method for parallel inverters

Conference Paper *in* PESC Record - IEEE Annual Power Electronics Specialists Conference · February 2004

DOI: 10.1109/PESC.2004.1355222 · Source: IEEE Xplore

CITATIONS
616

READS
7,440

7 authors, including:

Karel De Brabandere
3E
36 PUBLICATIONS **2,853** CITATIONS
SEE PROFILE

Jeroen Van den Keybus
KU Leuven
64 PUBLICATIONS **3,337** CITATIONS
SEE PROFILE

Achim Woyte
3E
74 PUBLICATIONS **3,949** CITATIONS
SEE PROFILE

Ronnie Belmans
KU Leuven
609 PUBLICATIONS **15,641** CITATIONS
SEE PROFILE

A Voltage and Frequency Droop Control Method for Parallel Inverters

K. De Brabandere, B. Bolsens, J. Van den Keybus, A. Woyte, J. Driesen and R. Belmans
K.U.Leuven ESAT / ELECTA
Kasteelpark Arenberg 10, 3001 Leuven, Belgium
email: Karel.DeBrabandere@esat.kuleuven.ac.be

***Abstract*— In this paper, a new control method for the parallel operation of one or several inverters in an island grid or the mains is described. Frequency and voltage control, including mitigation of voltage harmonics, are achieved without the need for any common control circuitry or communication between the inverters. Each inverter supplies a current that is the result of the voltage difference between a reference AC voltage source and the grid voltage across a virtual impedance with real and/or imaginary parts. The reference AC voltage source is synchronised with the grid, with a phase shift, depending on the difference between nominal and real grid frequency. A detailed analysis show that this approach has superior behaviour in comparison with the existing droop control methods, considering the mitigation of voltage harmonics, short-circuit behaviour and, in the case of a non-negligeable line resistance, the 'efficient' control of frequency and voltage. Experiments show the behaviour of the method for an inverter feeding a highly distorted load and during the connection of two parallel inverters in operation.**

I. INTRODUCTION

Frequency and voltage control in island grids, supplied by several inverters in parallel, can be obtained by means of various control methods, with or without communication. Control methods solely based on local measurements exhibit a superior redundancy as they do not rely on communication for reliable operation. A peculiar aspect of these methods is that they only have a proportional controller for frequency and voltage, lacking any forms of integral control. Control of a distributed system without use of communication can only be achieved at the price of permitting a small error. Therefore, these techniques are generally denoted as droop control methods [1]-[6]. The small droop is generally considered acceptable as long as the error remains within predefined limits. However, it should be noted that techniques are described in literature which extend the local droop control by a global integral control through low bandwidth communication, combining both redundancy and integral control. In this paper, only the local droop control, without use of communication, is elaborated. The global integral control may be regarded as a possible although not necessary extension to this method.

This paper starts with a review of the droop control method. Although this method, as described in literature, performs well for inductive lines, the performance in case of resistive lines is poor. In this paper, it is shown how the classical droop method can easily be adapted to account for the grid impedance, providing good performance under all conditions. A major benefit of this technique compared to existing methods [1]-[6] is especially prevalent in low-voltage cable grids, generally having a mostly resistive line impedance. In these grids, the proposed technique is appreciably more efficient in controlling frequency and voltage in proportion to the needed active and reactive power flows. Secondly, it is explained why the approach of controlling active and reactive currents instead of active and reactive powers exhibits some advantages, especially in case of a short circuit. Controlling any non-zero active or reactive power during short circuit (grid voltage equals zero) results in infinitely high currents, which is avoided when controlling the active and reactive current. Finally, a new approach to obtain voltage and frequency droop control is described. A complex finite-output impedance voltage source is imitated, by controlling the current, flowing through a virtual impedance as a result of the difference between a virtual ac power source and the grid voltage. In contrast to the classical droop control, the presented approach intrinsically controls not only the fundamental voltage and frequency, but also the harmonic components of the voltage, and is thus suited to supply highly distorted loads. A detailed analysis shows that, with exception of the additional harmonic control, the performance of this new approach is equivalent to the abovementioned droop control method through controlling active and reactive currents.

II. THEORY

A. Droop control through active and reactive power

The power flow into a line at point A, as represented in Fig. 1, is described as [7]:

$$\begin{aligned} P + jQ = \underline{S} = \underline{U}_1 \underline{I}^* &= \underline{U}_1 \left(\frac{\underline{U}_1 - \underline{U}_2}{\underline{Z}} \right)^* \\ &= U_1 \left(\frac{U_1 - U_2 e^{j\delta}}{Z e^{-j\theta}} \right) \\ &= \frac{U_1^2}{Z} e^{j\theta} - \frac{U_1 U_2}{Z} e^{j(\theta+\delta)} \end{aligned} \quad (1)$$

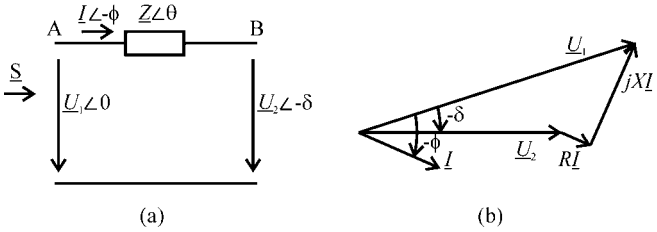

(a) (b)

Fig. 1: (a) Power flow through a line, (b) phasor diagram.

Thus, active and reactive power flowing into the line are described as:

$$P = \frac{U_1^2}{Z} \cos\theta - \frac{U_1 U_2}{Z} \cos(\theta + \delta) \quad (2)$$

$$Q = \frac{U_1^2}{Z}\sin\theta - \frac{U_1 U_2}{Z}\sin(\theta+\delta) \quad (3)$$

With $Ze^{j\theta}=R+jX$, (2) and (3) are rewritten as:

$$P = \frac{U_1}{R^2+X^2}\left[R(U_1 - U_2\cos\delta) + XU_2\sin\delta\right] \quad (4)$$

$$Q = \frac{U_1}{R^2+X^2}\left[-RU_2\sin\delta + X(U_1 - U_2\cos\delta)\right] \quad (5)$$

or

$$U_2\sin\delta = \frac{XP - RQ}{U_1} \quad (6)$$

$$U_1 - U_2\cos\delta = \frac{RP + XQ}{U_1} \quad (7)$$

For overhead lines $X >> R$, meaning that R may be neglected. If also the power angle δ is small, then sin δ = δ and cos δ = 1. Equations (6) and (7) then become:

$$\delta \cong \frac{XP}{U_1 U_2} \quad (8)$$

$$U_1 - U_2 \cong \frac{XQ}{U_1} \quad (9)$$

For $X >> R$, small power angle δ and small voltage difference U_1-U_2, (8) and (9) show that the power angle depends predominantly on P, while the voltage difference depends predominantly on Q. Or, in other words, the angle δ can be controlled by regulating P, while the inverter voltage U_1 is controllable through Q. Control of frequency dynamically controls the power angle and, thus, the real power flow. Thus, by adjusting P and Q independently, frequency and amplitude of the grid are determined. These conclusions form the basis for the well-known frequency and voltage droop regulation through respectively active and reactive power:

$$f - f_0 = -k_p(P - P_0) \quad (10)$$

$$U_1 - U_0 = -k_q(Q - Q_0) \quad (11)$$

f_0 and U_0 are nominal frequency and nominal grid voltage respectively, and P_0 and Q_0 are the (momentary) setpoints for active and reactive power of the inverter. The frequency and voltage droop control characteristics are shown graphically in Fig. 2.

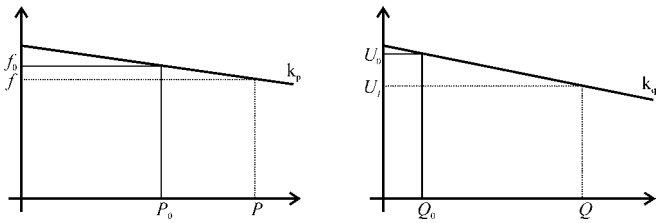

Fig. 2: frequency and voltage droop control characteristics.

As a first improvement in the proposed control scheme, R is no longer neglected. This is especially worthwile in low voltage cable grids, generally having a mostly resistive line impedance. Ultimately, X could be neglected instead of R. In this case, adjusting active power influences the voltage amplitude, while adjusting reactive power Q influences the frequency. Relationships have changed radically, in such a way that the droop regulation described by (10) and (11) will not be effective anymore.

In general, both X and R are considered. For this general case, the use of a linear rotational transformation matrix **T** from active and reactive power P and Q to modified active and reactive power P' and Q' is proposed by the authors:

$$\begin{bmatrix} P' \\ Q' \end{bmatrix} = \mathbf{T}\begin{bmatrix} P \\ Q \end{bmatrix} = \begin{bmatrix} \sin\theta & -\cos\theta \\ \cos\theta & \sin\theta \end{bmatrix}\begin{bmatrix} P \\ Q \end{bmatrix} = \begin{bmatrix} \frac{X}{Z} & -\frac{R}{Z} \\ \frac{R}{Z} & \frac{X}{Z} \end{bmatrix}\begin{bmatrix} P \\ Q \end{bmatrix} \quad (12)$$

Applying this transformation on equations (4) and (5) results in:

$$\sin\delta = \frac{ZP'}{U_1 U_2} \quad (13)$$

$$U_1 - U_2\cos\delta = \frac{ZQ'}{U_1} \quad (14)$$

For small power angle δ and voltage difference U_1-U_2, (13) and (14) show that the power angle depends only on P', while the voltage difference depends only on Q'. Or, in other words, the angle δ can be controlled by regulating P', while the inverter voltage U_1 is controllable through Q'. As the grid frequency is influenced through the angle δ, the definition of P' and Q' permits to independently influence frequency and amplitude of the grid. This is illustrated graphically in Fig. 3. The effect of P', Q', P and Q on voltage and frequency is illustrated for different ratios of inductivity X to resistivity R of the line impedance. To derive P' and Q', it suffices to know the ratio R/X. Knowledge of the absolute values of the line impedance is not needed.

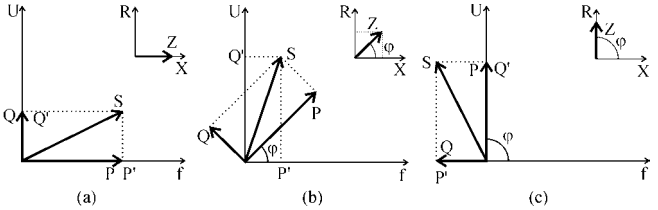

Fig. 3 Influence of active and reactive power on voltage and frequency for different line impedance ratios: (a) R/X=0, (b) R/X=1, (c) R/X=∞.

$\varphi=\pi-\theta$ is equal to the atan(R/X). From Fig. 3, it can be seen that for mainly inductive lines $P' \cong P$ and $Q' \cong Q$, while for mainly resistive lines $P' \cong -Q$ and $Q' \cong P$. If the ratio R/X is not known, a compromise may be to consider R and X to be equal.

The frequency and voltage droop regulation becomes:

$$f - f_0 = -k_p(P' - P_0') \quad (15)$$

$$U_1 - U_0 = -k_q(Q' - Q_0') \quad (16)$$

B. Droop control through active and reactive current

Active and reactive currents I_a and I_r through $\underline{Z}$ are:

$$I_a = \frac{P}{U_1} = \frac{R(U_1 - U_2\cos\delta) + XU_2\sin\delta}{R^2+X^2} \quad (17)$$

$$I_r = \frac{Q}{U_1} = \frac{-RU_2\sin\delta + X(U_1 - U_2\cos\delta)}{R^2+X^2} \quad (18)$$

Then, analogous to the modified active and reactive powers, active and reactive currents are defined as:

$$\begin{bmatrix} I_a' \\ I_r' \end{bmatrix} = \mathbf{T} \begin{bmatrix} I_a \\ I_r \end{bmatrix} \tag{19}$$

And thus:

$$I_a' = \frac{P'}{U_1} = \frac{U_2 \sin\delta}{Z} \tag{20}$$

$$I_r' = \frac{Q'}{U_1} = \frac{U_1 - U_2 \cos\delta}{Z} \tag{21}$$

As a variant to the previously described droop method, not the (modified) active and reactive powers, but the (modified) active and reactive currents I_a' and I_r' are controlled. The frequency and voltage droop control characteristics then become:

$$f - f_0 = -k_a \left(I_a' - I_{a,0}' \right) \tag{22}$$

$$U_1 - U_0 = -k_r \left(I_r' - I_{r,0}' \right) \tag{23}$$

This is shown graphically in Fig. 4.

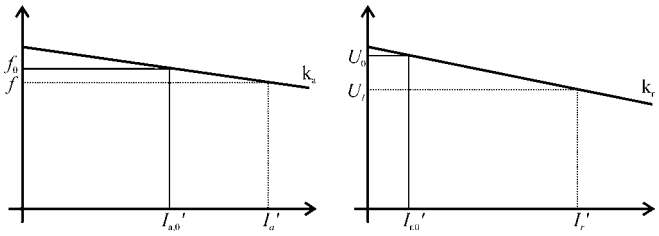

Fig. 4: Frequency and voltage droop characteristics as a function of modified active and reactive power.

This approach has benefits when U_1 differs significantly from its nominal value (e.g. when a short-circuit occurs at U_1). Implementing (15) and (16) would result in infinite currents during short-circuit (U_1 = 0), which are avoided when equations (22) and (23) are implemented.

C. Droop control through emulation of a finite-output impedance voltage source

In this section, a new approach to obtain voltage and frequency droop control is described. The purpose is to imitate the behaviour of a synchronous generator, connected to the grid. The synchronous generator is represented by a finite-output impedance voltage source (Thévenin equivalent), as shown left of the bar in Fig. 5. It consists of an AC voltage source $\underline{U}_0$ in series with an impedance $\underline{Z}_d$. The Thévenin equivalent is connected with the grid $\underline{U}_2$ through the line impedance $\underline{Z}$. $\underline{U}_1$ is the voltage at the point of coupling between $\underline{Z}_d$ and $\underline{Z}$. The grid, here represented by $\underline{U}_2$, may be the (stiff) mains, or a local stand-alone or island grid (microgrid), containing one or more inverters and/or rotating generators. To the best of the knowledge of the authors, the notion of a "virtual impedance" in this context is used only once before [8], where a purely ohmic resistance is considered.

1) Frequency droop

The Thévenin voltage source has the same frequency as the grid, but with phase angle difference ψ, proportional to the difference between real (measured) and nominal grid frequency:

$$\psi = -k_\psi \left(f - f_0 \right) \tag{24}$$

When the measured grid frequency is lower than the nominal grid frequency (e.g. 50 Hz in Europe), the phase angle is positive and $\underline{U}_0$ leads $\underline{U}_1$. When the measured frequency is higher, the phase angle is negative and $\underline{U}_0$ lags $\underline{U}_1$. This behaviour is denoted with the term frequency droop.

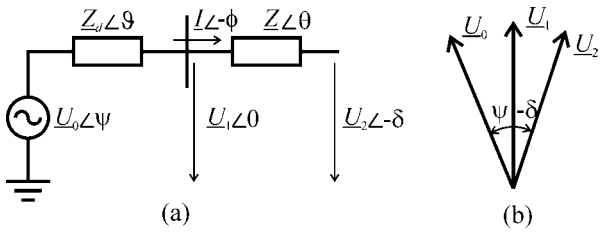

Fig. 5 Thévenin equivalent of a finite-output impedance voltage source in connection with a grid and load: (a) circuit and (b) phase diagram.

2) Voltage droop

The amplitude U_0 of the voltage source is assumed constant and equal to the nominal grid voltage amplitude U_{nom}. Voltage droop between $\underline{U}_0$ and the local grid voltage $\underline{U}_1$ occurs because of the series impedance $\underline{Z}_d$.

3) Choice of $\underline{Z}_d$ and k_ψ

The virtual impedance $\underline{Z}_d$ is equivalent to the series impedance of a synchronous generator. However, whereas the series impedance of a synchronous generator is mainly reactive, the virtual impedance may be chosen arbitrarily. In contrast to a real impedance, this virtual impedance represents no power losses, and thus it is possible to imitate the behaviour of a resistance, without compromising efficiency.

By analysing the equivalence of the new approach with the droop control method through active and reactive current, cfr. (22) and (23), an appropriate choice of $\underline{Z}_d$ and k_ψ could be made as a function of k_a and k_r. Hereto, modified active and reactive currents I_a' and I_r' through $\underline{Z}_d$ are calculated. The analysis is done, based on the assumption that there are no harmonics and only the fundamental frequency component is considered. This assumption enables to write the relationship between voltage and current of the virtual impedance using phasors:

$$I_a - jI_r = \underline{I} = \frac{\underline{U}_0 - \underline{U}_1}{\underline{Z}_d} = \frac{U_0 e^{j\psi} - U_1}{Z_d e^{j\vartheta}} \tag{25}$$

Knowing that $Z_d e^{j\vartheta} = R_d + jX_d$, this means:

$$I_a = \frac{R_d \left(U_0 \cos\psi - U_1 \right) + X_d U_0 \sin\psi}{{Z_d}^2} \tag{26}$$

$$I_r = \frac{-R_d U_0 \sin\psi + X_d \left(U_0 \cos\psi - U_1 \right)}{{Z_d}^2} \tag{27}$$

In the case that $\vartheta = \theta$, which means that $R_d/X_d = R/X$, transformation with **T** yields:

$$I_a' = \frac{U_0 \sin\psi}{Z_d} \tag{28}$$

$$I_r' = \frac{U_0 \cos\psi - U_1}{Z_d} \tag{29}$$

Based on (22), (23), (24), (28) and (29), and by assuming that $\sin\psi \cong \psi$ and $\cos\psi \cong 1$, the following equations for Z_d and k_ψ as a function of k_a and k_r are derived:

$$Z_d = k_r \tag{30}$$

$$k_\psi = \frac{k_r}{U_0 k_a} \tag{31}$$

A good strategy in determining $\underline{Z}_d$ and k_ψ, is therefore to obtain the desired k_a and k_r from Fig. 4, to calculate Z_d and k_ψ from (30) and (31), and to choose the ratio R_d/X_d equal to R/X of the line impedance.

From this analysis, it can be concluded that the approach of imitating a finite-output impedance voltage source, is equivalent to the droop control through controlling modified active and reactive currents, except for the additional benefit of intrinsically controlling as well the voltage harmonics through a droop characteristic. In comparison with the droop control method through controlling active and reactive power, described in literature [1]-[6], the approach exhibits, in addition to the voltage harmonics mitigation, benefits considering short-circuit behaviour and achieves (in the case of a non-negligeable line resistance) a more 'efficient' control of frequency and voltage.

4) Incorporating current offset

The scheme of Fig. 5 can easily be extended to incorporate an additional current source representing an offset active and/or reactive current $\underline{I}_0$ generated by the inverter (Fig. 6). The combination of the current source with the finite-output impedance voltage source may represent a typical distributed generation unit (i.e. the current source), with additional frequency and/or voltage regulation capabilities (i.e. the finite-output impedance voltage source).

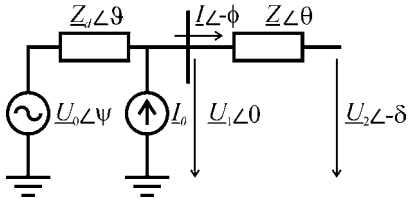

Fig. 6: Finite-output impedance voltage source with current source in parallel.

III. IMPLEMENTATION

The purpose of the control scheme is to emulate the behaviour described in section II.C by controlling the current and voltage output of a single phase PWM voltage source inverter with LCL output filter. In Fig. 7 both the virtual-system model of the finite-output impedance voltage source and the real-system model of the LCL output filter are shown. The output current i_{grid} and output voltage u_{grid} are measured, while the grid parameters on the right hand of the bar are unknown. This unknown grid may be the (stiff) mains, a microgrid, or a stand-alone load, meaning that the grid impedance may range from almost zero (stiff mains) up to infinity (no-load stand-alone). The control scheme should be able to control u_{grid} and i_{grid}, emulating the virtual-system model, irrespective of the grid impedance. However, because of practical reasons, in the subsequent development, capacitance voltage u_{cap} and i_{grid} instead of grid voltage u_{grid} and i_{grid} of the real-system model will be controlled to be equal to u_{grid} and i_{grid} of the virtual-system model.

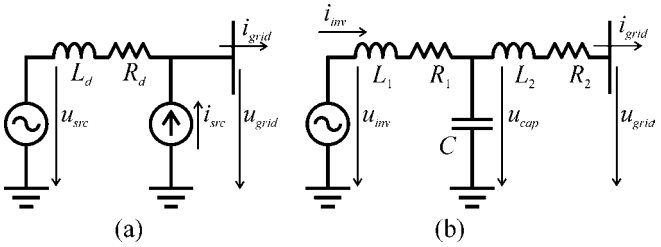

Fig. 7: (a) virtual-system model; (b) real-system model.

The overall control scheme, implementing the proposed voltage and frequency droop control method, is shown in Fig. 8. The control scheme is decomposed in two main parts. The rightmost part generates the virtual-system voltage source u_{src} by tracking the fundamental amplitude and frequency of the voltage u_{cap} and applying the phase shift ψ according to (24). The second part emulates the finite-output impedance, by calculating the inverter voltage u_{inv} that should be applied by PWM on the real system, based on the virtual-system voltage source u_{src} and measured values u_{cap} and i_{grid}. The implementation of these two parts is elaborated in the next subsections.

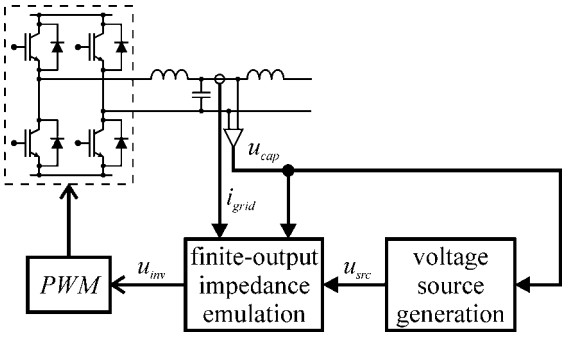

Fig. 8 Overall scheme for the proposed voltage and frequency droop control method.

A. Voltage source generation

Fig. 9 presents the full scheme to generate the reference voltage u_{src}, taking into account the measured value of u_{cap}. This scheme comprises two subparts, the first achieving fundamental voltage amplitude and frequency tracking, the other calculating the phase shift and amplitude of the virtual-system voltage source u_{src}.

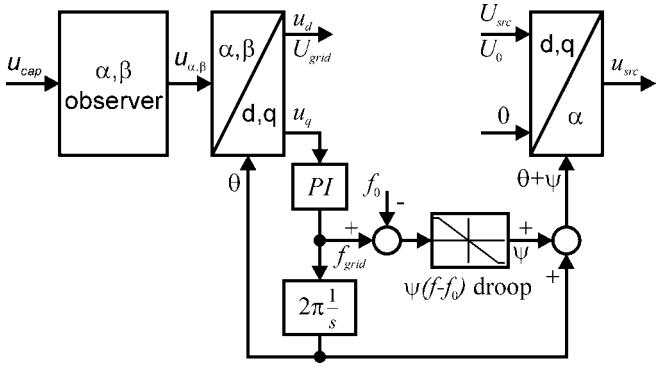

Fig. 9 Voltage source generation scheme.

1) Fundamental voltage amplitude and frequency tracking

Based on a single-phase grid voltage measurement u_{cap}, the fundamental voltage amplitude U_{grid} and frequency f_{grid} are estimated. To this extent the fundamental voltage is extracted by use of a Kalman estimator. The approach is based on a technique, described in literature, where it is used for voltage harmonics tracking [9]. The Kalman estimator observes, besides the fundamental component, also the 3rd, 5th, and 7th harmonic components. Observing these harmonics improves the tracking performance under distorted voltage conditions considerably. The fundamental output component is used further, represented by two values u_α and u_β, the former being in phase with u_{cap}, the latter representing the quadrature component. These components are named u_α and u_β, as they are equivalent to the components from the Clark tranformation in a three phase system. Subsequently, the Park transformation is applied, which results in u_d and u_q. The rotation angle θ for the Park transformation is obtained from a Phase Locked Loop (PLL), which regulates u_q to zero by use of a Proportional-Integral (PI) regulator [10]. As a result, u_d is equal to the amplitude U_{grid} of the fundamental voltage, while the frequency f_{grid} is a result from inside the PLL (Fig. 9). In Fig. 10, the fundamental voltage and frequency tracking of a distorted voltage waveform is illustrated in a simulation. In the simulation, the fundamental voltage is tracked in about 5 periods, while the initial error of u_d and u_q due to an initial phase shift of pi/2 is cancelled for in about the same time.

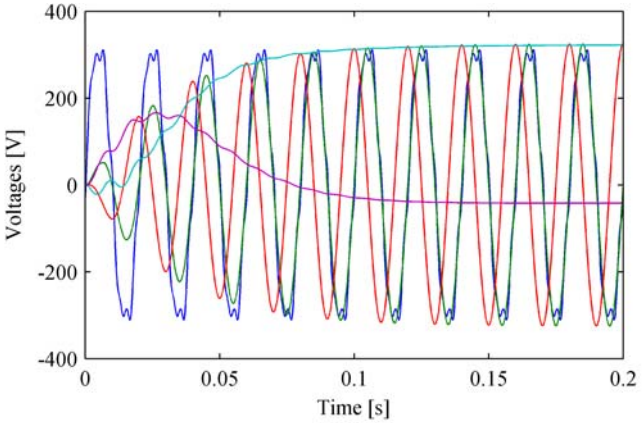

Fig. 10: Fundamental voltage and amplitude tracking: u_{cap} (blue), u_α and u_β (green and red), u_d and u_q (cyan and magenta).

2) Phase shift and amplitude calculation

Based on the estimated fundamental voltage amplitude U_{grid} and frequency f_{grid}, the amplitude U_{src} and the power angle ψ of the virtual-system voltage source u_{src} are calculated as being equal to:

$$\psi = -k_\psi \left(f - f_0 \right) \tag{32}$$

$$U_{src} = U_0 \tag{33}$$

Equations (32) and (33) are adjusted to account (approximately) for the limited current rating $I_{\max}$ of the inverter by ensuring that (not shown in Fig. 9):

$$U_{grid} - \left\| Z_d \right\| I_{\max} \le U_{src} \le U_{grid} + \left\| Z_d \right\| I_{\max} \tag{34}$$

$$\left| \psi \right| \le \min\left(\frac{\pi}{2}, \frac{\left\| Z_d \right\| I_{\max}}{U_0} \right) \tag{35}$$

Applying the inverse Park transformation on [U_{src} 0] with the rotation angle $\theta + \psi$ returns the sinusoidal voltage u_{src}.

B. Finite-output impedance emulation

The emulation of the finite-output impedance is obtained by the use of a hybrid voltage-current controller. Instead of having a current control loop for i_{grid} inside a voltage control loop for u_{cap} (or the other way round), both current and voltage are simultaneously controlled to emulate the finite-output impedance. This approach is necessary as the grid impedance is not known, and could vary from 0 to infinity. Stability problems would arise in a primary current control loop for very large grid impedances, while the same is true in a primary voltage control loop for very small grid impedances (see e.g. [2]). Different control methods can be used hereto, such as classical (e.g. root locus), modern (e.g. Linear Quadratic Gaussian (LQG)), robust (e.g. $\mathcal{H}_\infty$) or non-linear (e.g. adaptive) control methods. Here, the LQG optimal control approach is followed, using a Kalman estimator and a linear quadratic regulator.

The control scheme is shown in Fig. 11 and incorporates as well disturbance estimation and reference following [11]. The real-system plant model **R** is described in state-space domain by:

$$s\begin{bmatrix} i_{inv} \\ u_{cap} \\ i_{grid} \end{bmatrix} = \begin{bmatrix} -\frac{R_1}{L_1} & -\frac{1}{L_1} & 0 \\ \frac{1}{C} & 0 & -\frac{1}{C} \\ 0 & \frac{1}{L_2} & -\frac{R_2}{L_2} \end{bmatrix} \begin{bmatrix} i_{inv} \\ u_{cap} \\ i_{grid} \end{bmatrix} + \begin{bmatrix} \frac{1}{L_1} \\ 0 \\ 0 \end{bmatrix} \left[u_{inv} + w \right]$$

$$\begin{bmatrix} u_{cap} \\ i_{grid} \end{bmatrix} = \begin{bmatrix} 0 & 1 & 0 \\ 0 & 0 & 1 \end{bmatrix} \begin{bmatrix} i_{inv} \\ u_{cap} \\ i_{grid} \end{bmatrix} + \begin{bmatrix} 0 \\ 0 \end{bmatrix} \left[u_{inv} + w \right] \tag{36}$$

The virtual-system model is incorporated through the transfer function **V**:

$$e = \frac{Z_d}{Z_d + 1} \frac{u_{cap} - u_{src}}{L_d s + R_d} + \frac{Z_d}{Z_d + 1} \left(i_{grid} - i_{src} \right) \tag{37}$$

The disturbance w in (36) represents the input-equivalent disturbance, caused by the combination of the grid voltage u_{grid} and the reference signal u_{src} and i_{src}. In fact, w is a virtual signal applied at the control input which would produce the same steady state error e as the combination of the actual disturbance u_{grid} and the reference signals u_{src} and i_{src}. Both disturbances are persistent, as they are both composed of sinusoidal components, which means that they can be modeled and cancelled for. **W** represents the input-equivalent disturbance model, with d an arbitrary impulsive input. Besides the fundamental component, also the 3rd, 5th, 7th and 9th harmonic components are modelled.

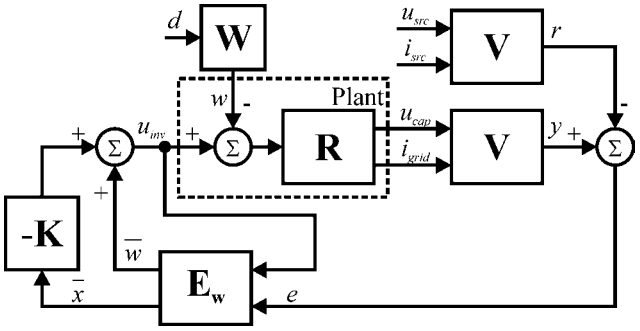

Fig. 11 LQG control scheme for the finite-output impedance emulation.

The Kalman estimator $\mathbf{E_w}$ estimates the states as well as the input-equivalent disturbance. The estimator is obtained by calculating the Kalman filter for the real-system plant model **R**, augmented with **V** and **W**, using the MATLAB function kalman.m.

The control law **K** is obtained by calculating the LQG optimal state-feedback gain of the real system model **R**, augmented only with **V** (**W** is not controllable), using the MATLAB function dlqr.m. The inverter voltage u_{inv} is obtained by augmenting the output of the control law with the estimate of the input-equivalent disturbance.

IV. Experimental Results

The control algorithm is converted from MATLAB /Simulink to 'C'-code using Real-Time Workshop. The code is then executed on a Texas Instruments 'C6711 Digital Signal Processor (DSP). An FPGA daughtercard on top of the 'C6711 DSK board generates the PWM signals for the IGBT PWM voltage-source inverter and provides an interface to the voltage and current measurements [12]. The total processor load is 81 % with the algorithm running at 9.2 kHz.

Using the setup of Fig. 12, experiments have shown the performance of the technique for resistive, inductive and capacitive loads and compact fluorescent lamps, the latter drawing a highly non-linear current. Also good results were obtained, during short-circuit operation and connection with the main grid. A second identical inverter setup is used to test the performance during parallel operation of two inverters.

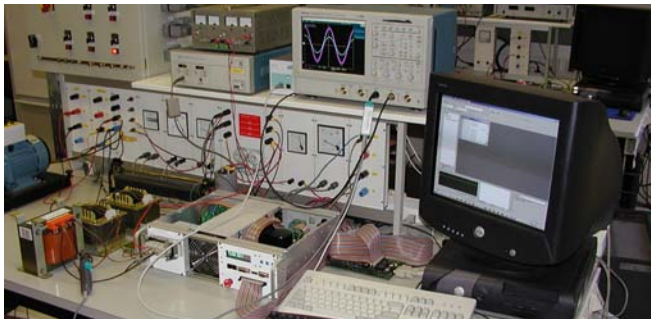

Fig. 12 Experimental setup of one of the two identical parallel inverters.

As a first example, demonstrating the steady-state behaviour, the supply of highly distorted load is considered. The inverter is operated in island mode, while the load consists of eight compact fluorescent lamps of different ratings. The virtual droop impedance is chosen to be equal to 1 Ω, with a ratio R_d/L_d equal to 4, while k_ψ is equal to 1 rad/Hz. As can be seen from Fig. 13, the voltage quality remains good, despite the very highly distorted nature of the current.

In a second example, two stand-alone grids were constructed, each consisting of one inverter supplying a resistive load. The experiment shows the parallel connection of both island grids during operation. The connection is obtained by first placing a 100 Ω resistance between both stand-alone grids, and gradually reducing this resistance in one second to 0 Ω. Fig. 14 shows the grid voltages and currents of both inverters during connection. The close-up graphs show the voltages and currents as they were shortly before and after connection. It can be seen that voltages synchronize smoothly, while the currents stabilize after a modest transient to almost perfect load sharing. Here, the droop impedance is chosen to be equal to 5 Ω, with a ratio R_d/L_d equal to 4, while k_ψ is equal to 1 rad/Hz.

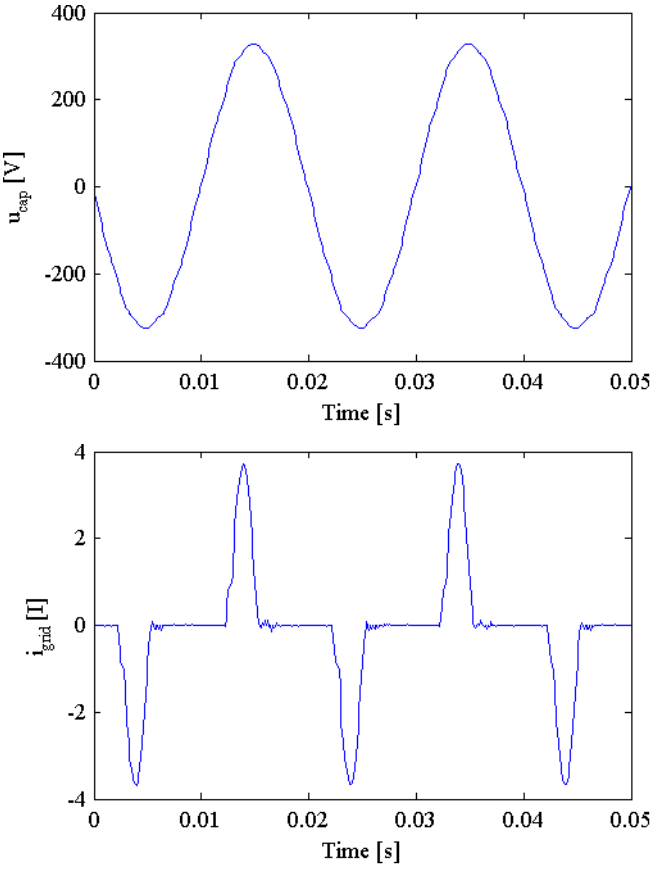

Fig. 13: Voltage and current waveforms feeding a highly distorted load with Z_d = 1 Ω.

V. Conclusion

A new method for controlling voltage and frequency in island grids using parallel inverters is presented. By imitating a voltage source with a complex finite-output impedance, voltage droop control is obtained. Frequency droop control results from synchronizing the power source with the grid, with a phase angle difference that depends on

the difference between nominal and real grid frequency. In comparison with existing techniques, the described method exhibits superior behaviour, considering the mitigation of voltage harmonics, the behaviour during short-circuit and, in the case of a non-negligeable line resistance, the 'efficient' control of frequency and voltage. Two experiments are included to show the described behaviour.

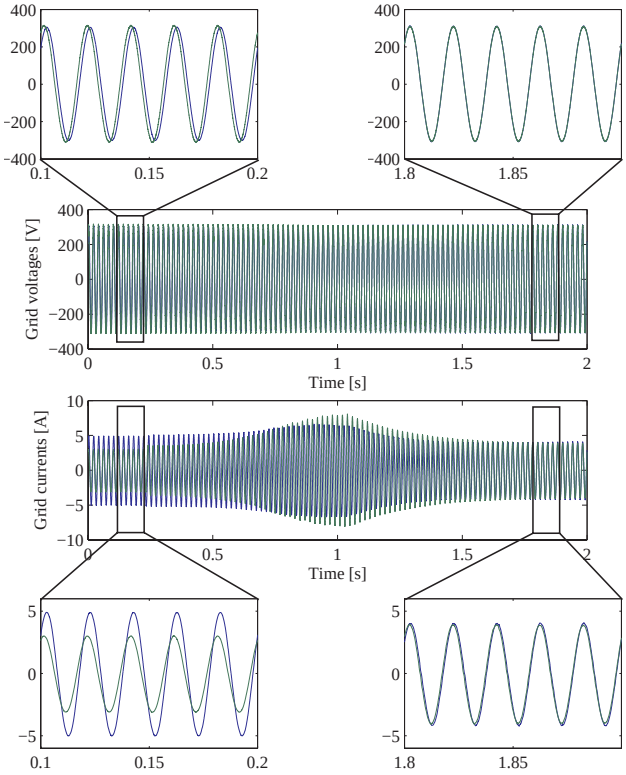

Fig. 14 Experimental grid currents and voltages before, during and after the connection during operation of two non-synchronized stand-alone grids.

ACKNOWLEDGMENT

The authors are grateful to the Belgian "Fonds voor Wetenschappelijk Onderzoek – Vlaanderen (FWO)" for its financial support, the Belgian "Instituut voor de aanmoediging van Innovatie door Wetenschap en Technologie in Vlaanderen (IWT)", for granting a GBOU research project on embedded generation and the European Commission for support through the FP5 Dispower project.

B. Bolsens holds a research scholarship of FWO, J. Van den Keybus held a research scholarship of IWT, and J. Driesen holds a postdoctoral research fellowship of FWO.

REFERENCES

[1] A. Tuladhar, H. Jin, T. Unger and K. Mauch, "Parallel operation of single phase inverter modules with no control interconnections," in *Proc. IEEE-APEC'97*, vol. 1, Feb. 1997, pp. 94-100.

[2] E. A. A. Coelho, P. C. Cortizo and P. F. D. Garcia, "Small-signal stability for parallel-connected inverters in stand-alone ac supply systems," *IEEE Trans. on Industry Applications*, vol. 38, no. 2, pp. 533-542, Mar./Apr. 2002.

[3] M. C. Chandorkar, D. M. Divan and R. Adapa, "Control of parallel connected inverters in standalone ac supply systems," *IEEE Trans. on Industry Applications*, vol. 29, no. 1, pp. 136-143, Jan./Feb. 1993.

[4] A. Engler, *Regelung von Batteriestromrichtern in modularen und erweiterbaren Inselnetzen*, PhD. Dissertation, Dept. Electr. Eng., Univ. Gesamthochschule Kassel, Kassel, Germany, 2001.

[5] M. Hauck and H. Späth, "Control of three phase inverter feeding an unbalanced load and operating in parallel with other power sources," in *Proc. EPE-PEMC'02*, Sept. 2002.

[6] C.-C. Hua, K.-A. Liao and J.-R. Lin, "Parallel operation of inverters for distributed photovoltaic power supply system," in *Proc. IEEE-PESC'02*, 23-27 March 2002.

[7] B. M. Weedy and B. J. Cory, *Electric Power Systems*, John Wiley & Sons, fourth edition, 1998.

[8] T. Skjellnes, A. Skjellnes, L. E. Norum, "Load sharing for parallel inverters without communication," in *Nordic Workshop on Power and Industrial Electronics*, Aug. 2002.

[9] A. A. Girgis, W. B. Chang and E. B. Makram, "A digital recursive measurement scheme for on-line tracking of power system harmonics," *IEEE Trans. on Power Delivery*, vol. 6, no. 3, pp. 1153-1160, July 1991.

[10] V. Kaura and V. Blasko, "Operation of a Phase Locked Loop system under distorted utility conditions," in *Proc. IEEE-APEC'96*, vol. 2, Mar. 1996, pp. 703-708.

[11] G. F. Franklin, J. D. Powell and M. Workman, *Digital Control of Dynamic Systems*, Addison Wesley Longman, third edition, 1998.

[12] J. Van den Keybus, *Development of a universal power measurement and control platform for low-voltage grid-coupled applications in a deregulated electricity market*, PhD. Dissertation, K.U.Leuven, Leuven, Dec. 2003.